A Journal of the Gesellschaft Deutscher Chemiker

Angewandte International Edition GDCh Chemie

www.angewandte.org

Accepted Article

Title: Photocatalytic Conversion of Methane to Ethane and Propane Using Cobalt-Cluster-Activated GaN Nanowires

Authors: Zhengwei Ye, Zhuoran Long, Bingxing Zhang, Ishtiaque Ahmed Navid, Jan Paul Menzel, Yifan Shen, Shubham Mondal, Facheng Guo, Theodore B. Norris, Victor S. Batista, and Zetian Mi

To be cited as: *Angew. Chem. Int. Ed.* **2025**, e202500158

Link to VoR: https://doi.org/10.1002/anie.202500158

WILEY VCH

10.1002/anie.202500158

WILEY VCH

RESEARCH ARTICLE

Photocatalytic Conversion of Methane to Ethane and Propane Using Cobalt-Cluster-Activated GaN Nanowires

Zhengwei Ye[a]†, Zhuoran Long[b]†, Bingxing Zhang[a]*, Ishtiaque Ahmed Navid[a], Jan Paul Menzel[b], Yifan Shen[a], Shubham Mondal[a], Facheng Guo[b], Theodore B. Norris[a]*, Victor S. Batista[b]*, Zetian Mi[a]*

[a] Z. W. Ye, B. X. Zhang, I. A. Navid, Y. F. Shen, S. Mondal, Prof. T. B. Norris, Prof. Z. Mi
Department of Electrical Engineering and Computer Science
University of Michigan, Ann Arbor
1301 Beal Avenue, Ann Arbor, MI 48109, USA
E-mail: bingxinz@umich.edu; tnorris@umich.edu; ztmi@umich.edu

[b] Z. R. Long, J. P. Menzel. F. C. Guo, Prof. V. S. Batista
Department of Chemistry
Yale University
2225 Prospect Street, New Haven, CT 06520, USA
E-mail: victor.batista@yale.edu

†These authors contribute equally.

Abstract: The photocatalytic nonoxidative coupling of methane (PNOCM) offers a promising route to synthesize valuable C_{2+} hydrocarbons while minimizing side reactions. Oxide-based photocatalysts have been predominant in this field, but suffering from limited conversion rates, selectivity, and durability due to poor C-C coupling as well as overoxidation of CH_4 by lattice oxygen. Here, we introduce an advancement in PNOCM for methane conversion into ethane and propane using GaN, one of the most produced semiconductors, together with trace amounts of metallic cobalt clusters (0.1 wt%). The photocatalytic system exhibits outstanding stability, maintaining performance over 110 hours, achieving conversion rates of approximately 192.3 mmol g^{-1} h^{-1} for ethane and ~17.9 mmol g^{-1} h^{-1} for propane, with virtually no coke byproducts detected, representing the highest activity and stability ever reported to our knowledge. This high activity is attributed to the critical methane activation and C-C coupling on Co cluster, which can be greatly accelerated via the ultrafast photogenerated charge transfer from p-GaN to Co cluster. Additionally, the GaN support further synergistically enhances methane activation by in situ generating N-H and O-H species under reaction, as well as provides a vital anti-overoxidation effect to CH_4 for high selectivity and stability.

Introduction

Methane (CH_4), a prevalent component of natural gas, methane hydrate, and shale gas reservoirs, has garnered significant attention owing to its extensive utilization as an energy resource and its crucial role as a fundamental precursor for synthesizing valuable chemicals in the realm of carbon chemistry [1]. As a result, the direct and selective transformation of CH_4 into high-value hydrocarbons (C_{2+} compounds) stands as a coveted objective in the chemical industry. Nevertheless, the inherent challenge lies in the inert, symmetric tetrahedral structure of CH_4, particularly in the initial dissociation of the formidable C–H bond (which demands 439.3 kJ mol^{-1} for breaking), a pivotal step for methane activation [2]. Within the domain of methane conversion, four primary pathways have been explored, including dry reforming, steam reforming, partial oxidation, and the carbon-carbon (C-C) coupling reaction. Among these, the C-C coupling reaction has garnered significant attention due to the formation of more valuable products with high energy density. The C-C coupling reaction can occur in two distinct forms: with involvement of oxidative agents (termed oxidative coupling of methane, OCM) [3], or without them (known as non-oxidative coupling of methane, NOCM) [4]. However, reactions involving oxidative agents often yield products that are more reactive than methane itself, leading to lower product selectivity and higher coke rate.

The non-oxidative coupling of methane (NOCM) involves a formidable thermodynamic barrier, and thus requires a considerable energy input to initiate the C-C coupling process. Conventionally, the prevailing approach to surmount this energy barrier has been the application of elevated temperatures [5]. In contrast, the photocatalytic non-oxidative coupling of methane (PNOCM) is driven by photon energy rather than thermal energy, so it can initiate the conversion of methane into higher order hydrocarbons and hydrogen under mild conditions. Such an approach has been demonstrated over large bandgap semiconductors, including titanium oxide, and tungsten oxide decorated with co-catalysts [3b, 6]. By employing this approach, the need for high reaction temperatures is by-passed, thereby decreasing energy consumption, minimizing coke formation, and reducing catalyst deactivation. Such advances have been substantiated through both photoelectrochemical systems and a photo-driven redox reaction cycle system [7]. While many prior reports have encountered challenges associated with low stability, limited production rates relative to catalysts consumption, and significant CO_2 production, one paramount challenge remains to develop an efficient photocatalytic system for PNOCM.

Another challenge lies in uncovering the fundamental molecular mechanisms. To investigate the methane activation and coupling across a variety of catalytic systems, density functional theory (DFT) simulations have been extensively utilized [5b, 8]. Methane activation by stepwise dissociation of C-H bonds

and formation of adsorbed CH_{4-n} (n = 1, 2, 3, 4) species initiates NOCM, PNOCM, and other methane conversions [9]. It is typically regarded as the rate-determining step and the reaction barrier can be overcome or reduced by photoexcitation [8j, 8k, 9d, 9e]. CH_2 and CH species provides building blocks for higher order products than C_2, while the complete dehydrogenation of methane to carbon leads to coke formation [8c, 8e]. Therefore, controlling the methane activation by proper catalytic system design and optimized reaction conditions can regulate product selectivity and coke resistance. Following the methane activation, C-C coupling via surface catalysis involves the binding of two CH_{4-n} species to the same or neighboring catalytic sites, which could be a critical part of the overall reaction [8l, 8m] compared to methane activation. C-C coupling products like ethylene can also undergo further reactions which yields side products like acetylene or benzene [5b, 8b, 8f]. Besides the option of eliminating these side reactions to enhance selectivity, it has also been demonstrated that these side reactions can be strategically harnessed to predominantly produce benzene within a zeolite environment [8n].

Herein, we report a scalable, wafer-based photocatalytic methane non-oxidation process for highly selective ethane and propane production by metallic Co cluster-loaded *p*-type GaN nanowires (Co/GaN) (**Figure 1a**). Under irradiation, the photocatalyst demonstrated high productivity, yielding 192.3 mmol g^{-1} h^{-1} of ethane and 17.9 mmol g^{-1} h^{-1} of propane with a high selectivity of 90.6% towards C_{2+} products. Notably, the photocatalyst also displayed stability over 110 hours with virtually no coke byproducts detected. Isotopic labeled experiments confirmed the methane conversion to ethane and propane process. We demonstrated that methane activation, C-C coupling, and hydrogen evolution reaction proceeds on Co sites, which are significantly accelerated by the ultrafast charge transfer from p-GaN to Co cluster during photocatalysis, and synergistically promoted by the in situ formed N-H and O-H species on GaN surface. The methane overoxidation by lattice oxygen and surface photocorrosion of semiconductor can be intrinsically suppressed due to the ultra-stable p-GaN nanowires, enabling the high durability of PNOCM process.

Results and Discussion

The magnesium-doped p-type GaN nanowires with high crystallinity and nonpolar lateral surfaces were synthesized using plasma-assisted molecular beam epitaxy (PAMBE) [10]. Field emission scanning electron microscopy (FESEM) images (**Figure 1b**) show that they have a length of ~1 μm and are well arrayed on a silicon wafer. The GaN forms a nitrogen polar wurtzite structure (**Figure S1**). The nanowires were then decorated with cobalt clusters (0.1 wt%) by photo-deposition, denoted as $Co_{0.1}$/GaN. X-ray diffraction (XRD) pattern (**Figure S2**) confirms that the crystal structure of nanowires corresponds to hexagonal GaN. A well-defined photoluminescence emission peak at 365 nm corresponding to the band edge emission of GaN can also be observed for the $Co_{0.1}$/GaN sample (**Figure S3**). Energy dispersive X-ray (EDS) elemental mapping further provides a clear visualization of the distribution of Co clusters on the GaN nanowire surfaces (**Figure 1c**). Furthermore, high-angle annular dark-field scanning transmission electron microscopy (HAADF-STEM) images (**Figure 1d, e**) indicate that the Co cluster on GaN nanowire surface show a typical lattice distance of 0.206 nm, corresponding to the Co hcp (1 $\bar{1}$ 0 1) facet**,** which serve as cocatalysts in photocatalytic processes [11]. Notably, GaN exhibits distinct lattice fringes with a width of 0.259 nm along the growth direction (c-axis) of the nanowires. High-resolution X-ray photoelectron spectroscopy (XPS) for GaN and $Co_{0.1}$/GaN were further performed (**Figure 1f**, **g**). The binding energy of Ga 3d and N 1s electrons in $Co_{0.1}$/GaN exhibited a negative shift compared to pristine GaN, resulted from the strong interaction of cocatalysts on GaN nanowires [12]. Co^0 metal species at 777.4 eV reveals the presence of metallic cobalt on GaN surface (**Figure 1h**) [13]. The post-reaction sample was obtained after 12 hours reaction and showed a 0.9 eV shift to 780.2 eV in Co 2p XPS spectra, due to the adsorption of oxygen species and stronger binding pattern on GaN surface during the photocatalytic redox process.

In the PNOCM reaction, a wafer loaded with the photocatalyst was immersed in deionized water with CH_4 used as the feed gas and irradiated by a 300W Xenon lamp. The controlled experiments (**Figure 2a**) indicate that $Co_{0.1}$/p-GaN exhibited the highest rates of ethane production (192.3 mmol g^{-1} h^{-1}) and propane production (17.9 mmol g^{-1} h^{-1}). Additionally, hydrogen was generated at a rate of 230.7 mmol g^{-1} h^{-1}, while the rate of carbon dioxide generation remained relatively low at 1.8 mmol g^{-1} h^{-1}. The majority of the hydrogen was generated through the non-oxidative methane coupling reaction, while a small portion resulted from the water splitting reaction (~2.5 mmol g^{-1} h^{-1}). These two rates were directly calculated based on the stochiometric ethane and propane to hydrogen ratio. On the contrary, the undecorated p-GaN and cobalt decorated silicon only showed limited ability of water splitting under illumination, suggesting the high NOCM activity is only derived from the $Co_{0.1}$/GaN. Additionally, the control groups with no light, methane or water individually exhibited no ability to drive any reaction. A control group without magnesium-doped intrinsic GaN exhibited the lack of such ability and a mere portion of hydrogen produced (**Figure S4**). To exclude the potential oxidation effects from the water molecules, a designated half reaction experiment was conducted with isopropanol (IPA) as the sacrificial agents, to consume the OH▪ radical group [14]. In **Figure S5**, alongside the comparison group with no IPA and no feed stock gas (CH_4), the process could be considered as the non-oxidative coupling reaction since the reaction proceed normally with the absence of OH▪ radical group.

10.1002/anie.202500158

RESEARCH ARTICLE

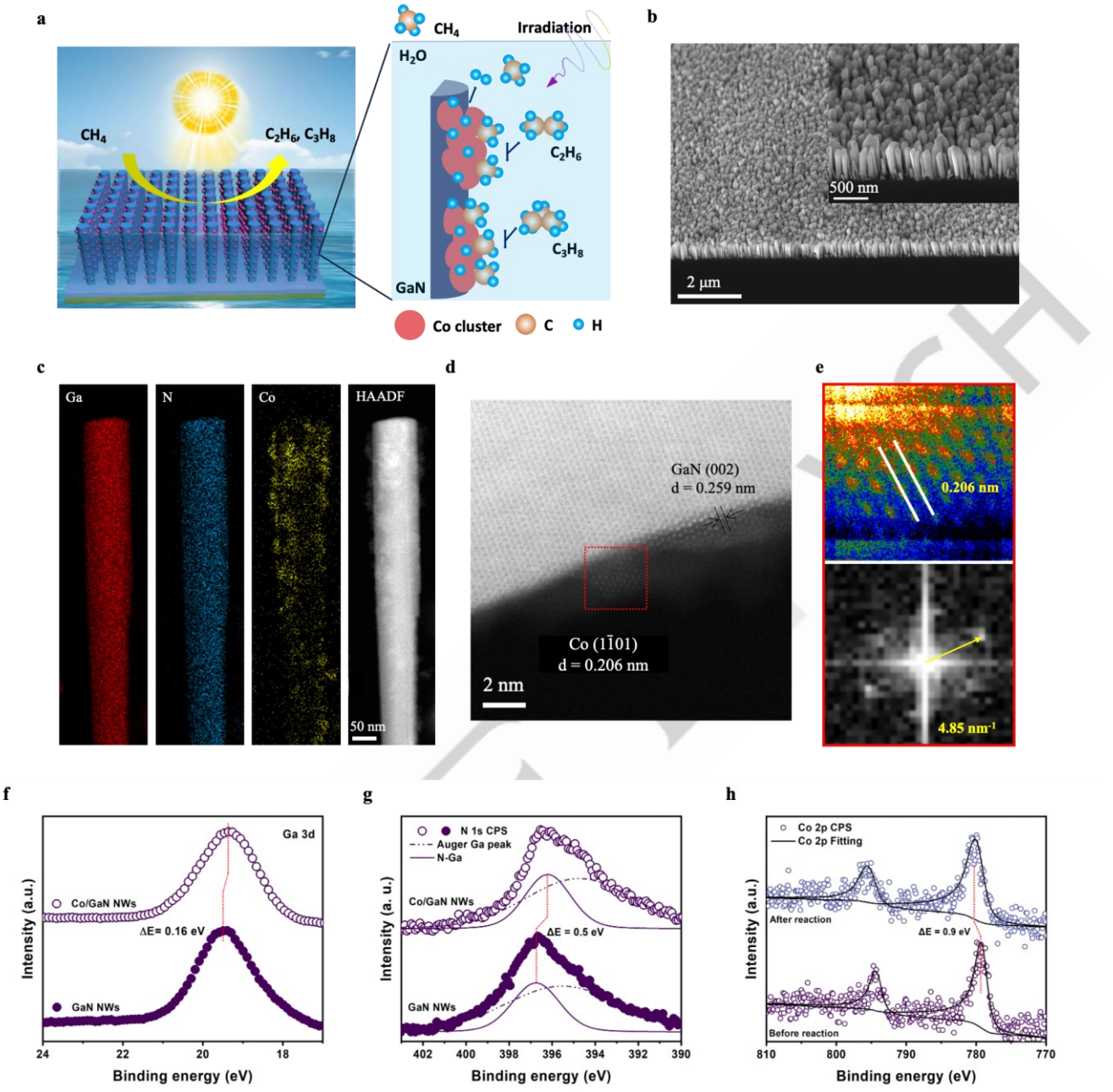

Figure 1. (a) Schematic illustration of non-oxidative methane coupling reaction into ethane and propane. (b) 45°-tilted FESEM image of magnesium doped GaN nanowires grown on silicon wafer with cobalt loading. (c) High-resolution HAADF-STEM images, EDS elemental mapping of one intact GaN nanowires with 0.1wt% cobalt cocatalysts loading. (d) Atomic-resolution HRSTEM image of cobalt loaded GaN surface. The red marked area indicated one cobalt cluster. (e) Reverse Fourier transform and Fourier transform of red marked area in (d). High-resolution XPS spectra of Ga 3d (f) and N 1s (g) states in $Co_{0.1}$/p-GaN NWs and GaN NWs. (h) Co 2p in $Co_{0.1}$/p-GaN NWs before and after NOCM reaction.

We then conducted an in-depth analysis of the impact of varying Co loading on the Co/GaN photocatalysts, with the designation 'x wt.%' representing the weight percentage of Co relative to GaN (**Table S1**). **Figure 2b** illustrates the production of alkanes displayed a characteristic volcano-like trend as the Co loading increased, reaching its zenith at $Co_{0.1}$/p-GaN with a high rate of 192.3 mmol g^{-1} h^{-1}. Beyond this optimal point, further increasing the Co loading led to a decline in photocatalytic performance. The intriguing results mean that a very small amount of Co content (≤ 0.1 wt%) is sufficient and favorable for PNOCM reaction. It can be attributed to the balanced cobalt cluster size and density and an optimal coupling with GaN NWs, which maximize the number of active sites (**Figure S6-9**) [15]. These results underscore the synergistic optimization of activity and selectivity for photocatalytic conversion of CH_4 triggered by trace Co clusters on p-GaN nanowires. For the factor of light

10.1002/anie.202500158

intensity (**Figure 2c**), elevating the light intensity led to a progressive augmentation of alkane production, culminating at 6 W cm^{-2}. Under this condition, ethane production soared to 192.3 mmol g^{-1} h^{-1}, representing a 6.8-fold increase compared to 28.2 mmol g^{-1} h^{-1} measured under the 1 W cm^{-2} condition. This observed augmentation in catalytic efficacy can be ascribed to the exceptionally efficient segregation and translocation of charge carriers at the interface of the photocatalyst [16].

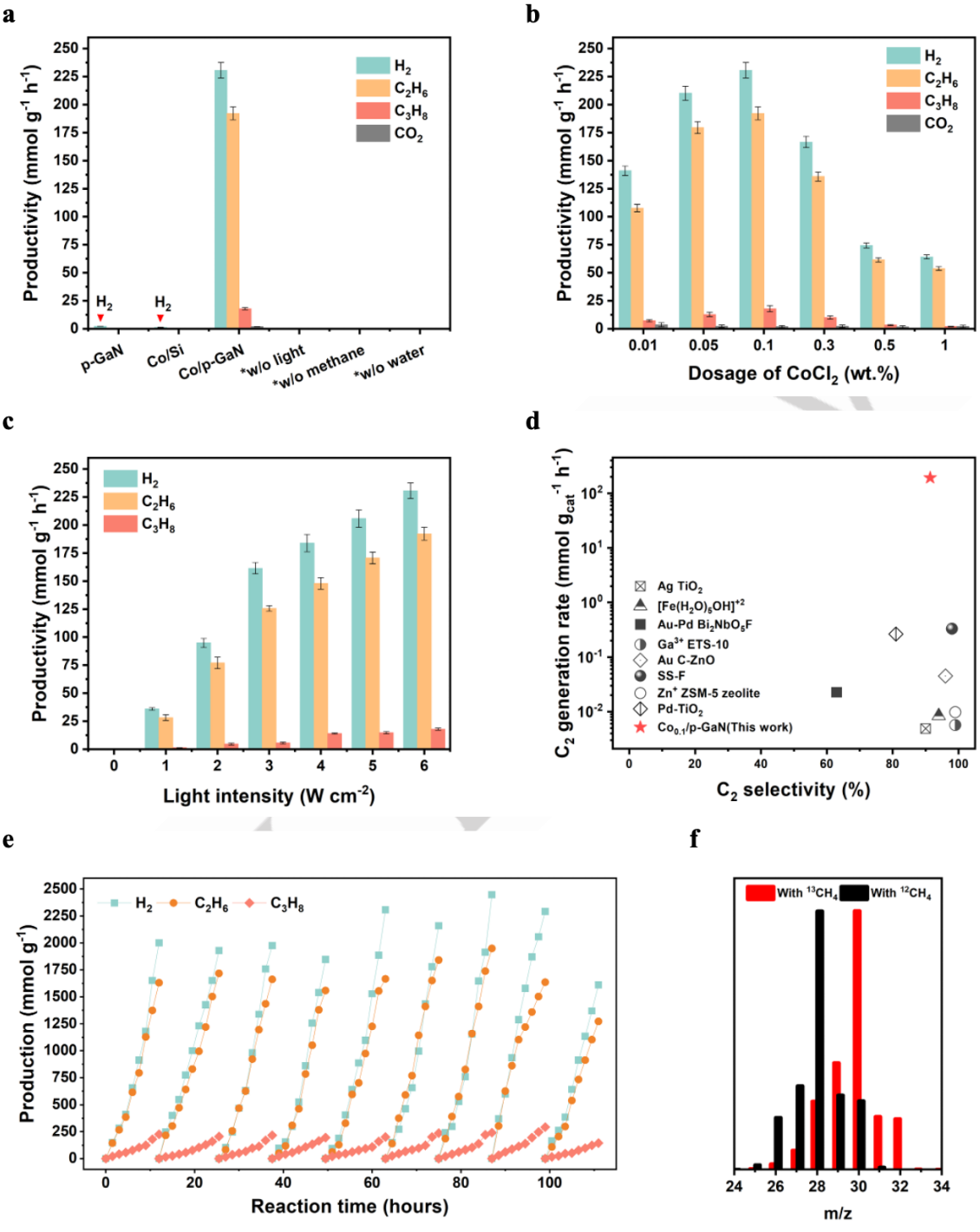

Figure 2. (a) PNOCM performance with no cocatalysts on p-GaN (magnesium doped GaN nanowires wafer), cobalt deposited silicon (111) wafer, cobalt deposited p-GaN, and the situations without light, methane, or water for $Co_{0.1}$/p-GaN. PNOCM performance by tuning (b) cobalt precursor dosage during synthesis and (c) light intensity. (d) Comparison in C_2 product selectivity and generation rate of $Co_{0.1}$/p-GaN for the photocatalytic NOCM with some previously reported photocatalysts. (e) Stability tests over $Co_{0.1}$/p-GaN. The reaction conditions include 0.66 cm^2 photocatalyst, 50 ml distilled H_2O, 1 atm CH_4, and 6 W cm^{-2}. (f) Ethane isotope GC-MS test results from ^{12}C and ^{13}C labelled methane feed gas.

10.1002/anie.202500158

RESEARCH ARTICLE

In a comparative analysis, summarized in **Figure 2d** and **Table S2**, the ethane production rate achieved by $Co_{0.1}$/GaN is nearly three orders of magnitude higher than previously reported results. The unprecedentedly high conversion rate of methane can be attributed to following reasons: 1) The ultrafast transfer of charge carriers from GaN to the lateral surface and Co clusters for efficient surface reaction, which will be revealed by the following PL analysis; 2) The ultrasmall cobalt cluster endows maximized exposure of highly intrinsic active sites; 3) The nanowire array structure significantly enhances the area-to-volume ratio, boosting the kinetics of interfacial reactions and mass transport of reactants while still allowing for unimpeded transport between cluster surface to solution [17]. Notably, the photocatalyst also exhibited impressive stability more than 110 hours (**Figure 2e**). The turnover number (TON) reached an exceptional value of 1571.1 during this stability test. Notably, our analysis of the sample after the stability test revealed no observable changes in the crystal structure of GaN (**Figure S10**). This can be attributed to the ultra-stable p-GaN nanowires with N-termination and high crystallinity by molecular beam epitaxy growth, which is confirmed by the STEM analysis (**Figure S1**) and consistent with our previous work [18]. Due to this characteristic, the methane overoxidation by lattice oxygen and surface photocorrosion of semiconductor can be intrinsically suppressed. The diminished activity over time to the end was primary attributed to the loss of Co cluster from the GaN surface, as shown by the STEM images (**Figure S10c**) and the Co 2P XPS spectra after 12-h reaction (**Figure 1h**). It is worth emphasizing the stability here is the highest among reported photocatalytic methane conversion systems to our knowledge (**Table S2**).

To provide evidence for the origin of the C_{2+} products, we conducted an isotopic test using ^{13}C-labelled methane (**Figure 2f**), which unambiguously showed the product of $^{13}C_2H_6$, providing solid evidence that the C_{2+} products are indeed originated from the nonoxidative coupling of methane feed gas.

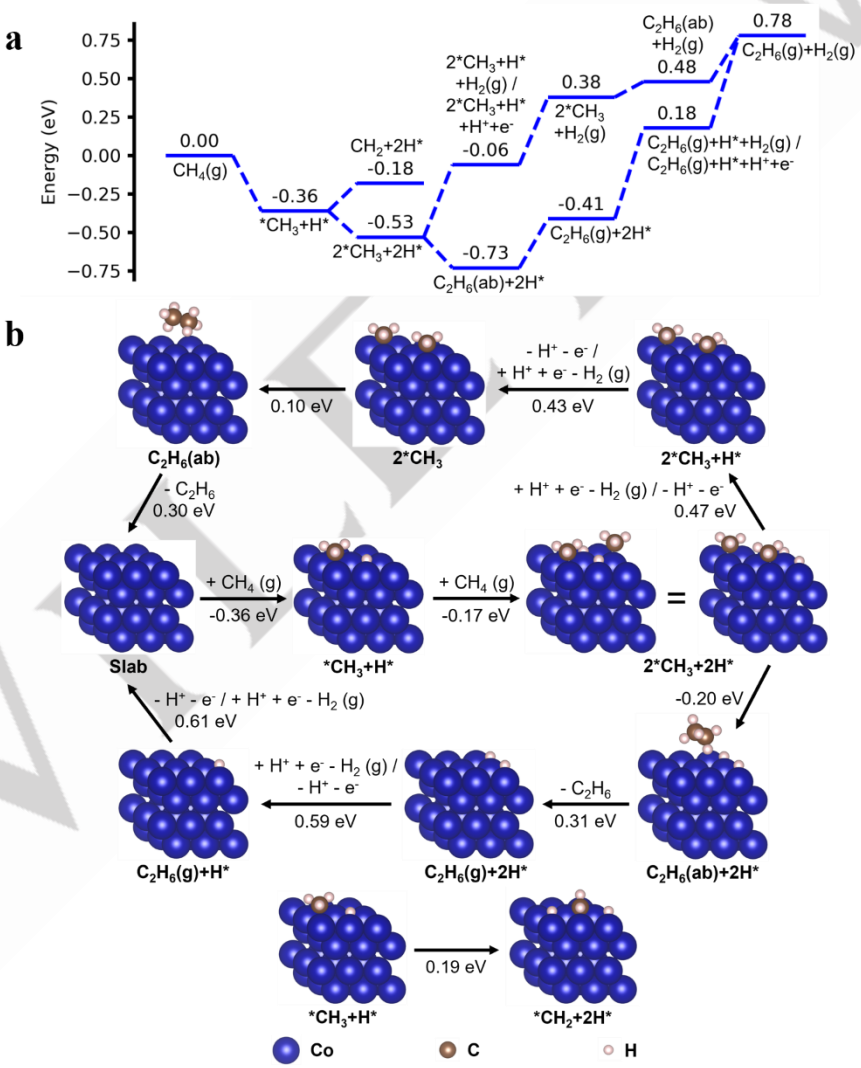

Figure 3. (a) Energy diagram and (b) reaction scheme for methane activation, C-C coupling and hydrogen evolution on a 3 × 3 × 4 slab of the Co [0001] surface as described by density functional theory calculations. The values in (a) are system energy relative to the starting state in eV. The equal sign in b) holds since the slab model is periodic. Key color code: Co (blue), C (brown), and H (white). All numbers are rounded to two decimal places.

10.1002/anie.202500158

RESEARCH ARTICLE

We then investigated the reaction mechanism of the ethane production from PNOCM using density functional theory (DFT). The calculations suggested specific roles played by the Co cocatalyst and GaN nanowires in the reaction mechanism. We modeled the Co cocatalyst surface by using a 3 × 3 × 4 slab of the Co hcp (0 0 0 1) surface. Previous works have suggested that methane activation can be achieved through generating •OH radicals, and then the •OH radicals can extract a hydrogen form the methane and produce •CH_3 radical [19]. However, from our computation results, while water can be dissociatively adsorbed to Co, releasing •OH radical from Co surface is energetically unfavorable (**Figure S11**). Instead, methane activation occurs through direct dissociative adsorption of CH_4, forming *CH_3 and H* adsorbate (here '*' denotes the adsorbed species). This dissociative adsorption is exothermic, releasing 0.36 eV of energy (**Figure 3**). We note that 'neglecting' the dispersion correction would give only 0.11 eV, consistent with a previous study which reported 0.14 eV.[8a] Further dissociation of *CH_3, resulting in *CH_2 and an additional H*, requires 0.19 eV, favoring selective ethane evolution over propane or higher hydrocarbons. The dissociation of a second CH_4 molecule releases 0.17 eV. Coupling two *CH_3 groups to form an adsorbed C_2H_6 is again exothermic and releases 0.20 eV (see the bottom route in **Figure 3a** and **3b**). Desorption of C_2H_6, requires 0.31 eV which can be supplied by the aforementioned methane activation and C-C coupling reaction. Hydrogen evolution from the two adsorbed H* species by thermal desorption would be energetically demanding (ΔE = 1.20 eV). However, this process can also be accomplished electrochemically, as follows:

$2\,H^* \rightarrow H^* + H^+ + e^-$, ΔE = 0.59 eV

$H^* + H^+ + e^- \rightarrow H_2(g)$, ΔE = 0.61 eV

or

$2\,H^* + H^+ + e^- \rightarrow H^* + H_2(g)$, ΔE = 0.59 eV

$H^* \rightarrow H^+ + e^-$, ΔE = 0.61 eV

The corresponding redox reactions involve electrons and holes generated on the GaN nanowire under light illumination. Similarly, in the top route in **Figure 3a** and **3b**, these two electrochemical hydrogen evolution steps with two *CH_3 adsorbates on the surface demand 0.47 and 0.43 eV, respectively. For the final C-C coupling of the remaining two *CH_3 groups, a mere 0.10 eV is needed, and the desorption of C_2H_6 demands 0.30 eV. Overall, methane activation on the Co slab is spontaneous, the C-C coupling reaction is thermodynamically favored, and the electrochemical hydrogen evolution requires a modest overpotential.

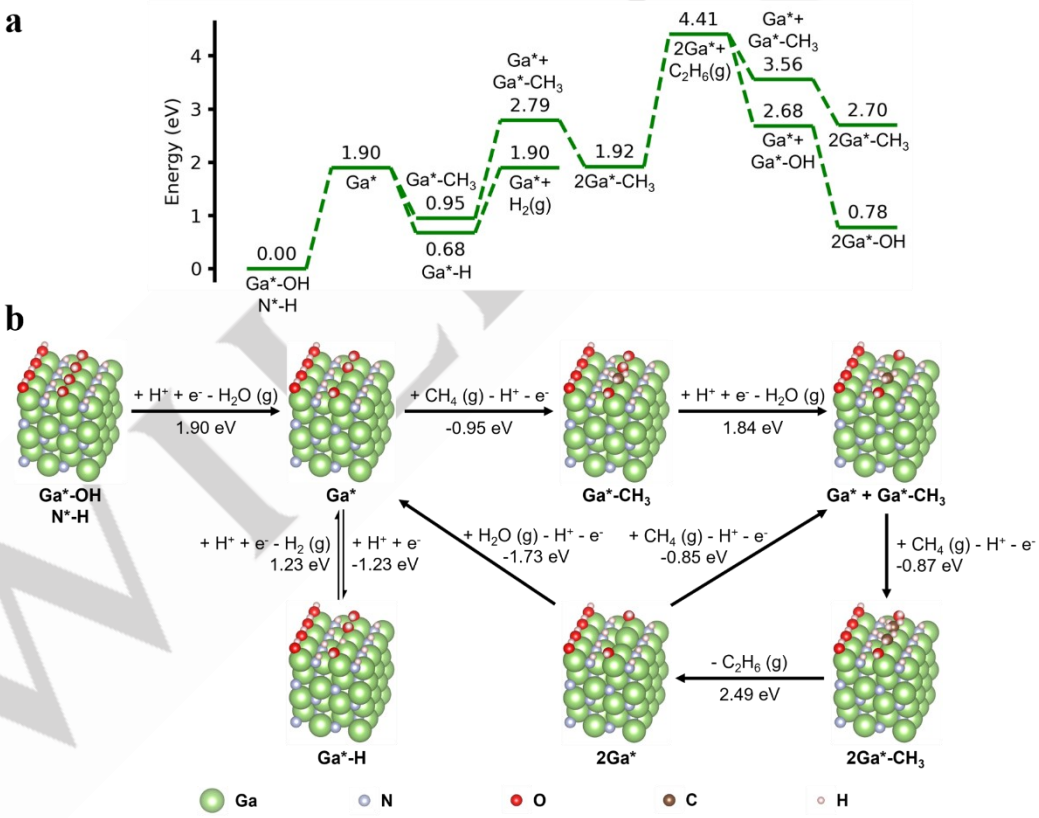

Figure 4. (a) Energy diagram and (b) reaction scheme for methane activation, C-C coupling and hydrogen evolution on a 2 × 4 × 4 slab of the GaN [$1\bar{1}00$] surface, as described by density functional theory calculations. Ga* and N* refer to the surface Ga and N atoms, correspondingly. The values in (a) are system energy relative to the starting state in eV. Key color code: Ga (green), N (grey), O (red), C (brown) and H (white). All numbers are rounded to two decimal places.

Our GaN nanowire model surface involved a 2 × 4 × 4 slab of the GaN n-plane [$1\bar{1}00$]. While a previous work on TiO_2 proposed that •OH radicals can be formed with radicals on TiO_2 surface [19a], our recent work shows radical formation on GaN surface is unfavorable.[20] Furthermore, •OH radicals and methane could lead to production of methanol [21]. which is not observed in our experiments. Overall, methane activation through production of •OH radicals can be excluded. DFT calculations show that the dissociative adsorption of CH_4 on GaN is exothermic, forming Ga*-CH_3 and N*-H (where Ga* and N* are surface Ga and N atoms, respectively) by releasing 1.58 eV of energy. The corresponding estimate without including the dispersion correction predicts a release of 1.31 eV, closely aligned with a previously reported estimate of 1.06 eV.[8d] Although a surface completely covered by Ga*-CH_3 and N*-H releases 1.43 eV energy per CH_4, dissociative adsorption of water is more favorable forming Ga*-OH and N*-H with a release of 2.43 eV per water molecule. Therefore, it is expected that the GaN surface is predominantly covered by Ga*-OH and N*-H. Under such conditions, methane conversion into ethane or propane is unfavored since methane activation would require opening a coordination site by thermal (**Figure S12**) or electrochemical (**Figure 4**) processes that are thermodynamically demanding. For example, generating a Ga* coordination site electrochemically, would involve the following process (**Figure 4**):

Ga*-OH + H^+ + e^- → Ga* + H_2O (g), Δ*E* = 1.90 eV

while methane activation at the open Ga* site would involve the following process:

CH_4 (g) → Ga*-CH_3 + H^+ + e^-, Δ*E* = -0.95 eV

For ethane formation, electrochemical elimination of the *OH next to a *CH_3 adsorbate would require 1.84 eV, while dissociating methane on that Ga* site would release 0.87 eV. In total, 0.95 eV would be required to exchange one Ga*-OH by Ga*-CH_3, and 1.92 eV be required to replacing two neighboring Ga*-OH. Moreover, C-C coupling of two neighboring Ga*-CH_3 to evolve C_2H_6 would require 2.49 eV. These substantial energy needs rule out methane activation and C-C coupling on the GaN surface, consistent with our experimental observation that pristine GaN nanowires do not catalyze methane activation. Only when decorated with Co cocatalyst, ethane evolution is observed. Nevertheless, to close the catalytic circle, the two vacant Ga* sites resulting from the C-C coupling can either dissociate water to revert the system to its initial state, or dissociate methane in preparation for the subsequent C-C coupling reaction. The hydrogen evolution on GaN is accomplished through the formation of Ga*-H electrochemically, as follows:

Ga* + H^+ + e^- → Ga*-H, Δ*E* = -1.23 eV

Ga*-H + H^+ + e^- → Ga* + H_2(g), Δ*E* = -1.23 eV

Therefore, we conclude that the functional role played by GaN nanowires is not to directly participate in the PNOCM, but instead to ultrafast supply electrons and holes to the Co cocatalyst. The density of state (DOS) of a model system (**Figure 5b**) is shown in **Figure 5a** (zoomed-in near the Fermi level, **Figure S13**). Photoabsorption by GaN excites electrons to the GaN conduction band minimum (CBM, ~ 0 eV) and generates holes in the GaN valence band maximum (VBM, ~ -1 eV). The strong orbital overlap among Co, Ga and N orbitals in the GaN band gap confirms the strong interaction between GaN and Co clusters for efficient charge transfer to Co clusters.

The computation on the Co_7-GaN cluster model was also performed (**Figure S14**). The dissociative adsorption of methane is still favorable, suggesting the same catalytical function of methane activation of the Co/GaN interface as the Co surface. The low coordinated environment at the Co/GaN interface makes the methane dissociative adsorption more energetically favorable than on Co surface, which, however, also makes the release of ethane/hydrogen evolution reaction more energetically demanding, reducing the likelihood of this region to participate in these reactions. Considering the cluster size around 2 nm with most exposed facets, the selected cobalt slab as the typically accessible active sites for simulation can well reveal the PNOCM process on the $Co_{0.1}$/GaN system (**Figure 3**).

The femtosecond ultrafast photoluminescence spectra were performed to detect the charge transfer on our GaN-based photocatalysis system. The time-resolved photoluminescence (TRPL) measurement shows a dramatic decay within several picoseconds for pristine p-GaN and $Co_{0.1}$/p-GaN **(Figure 5c)**, with a decay time of 3.1 and 4.96 ps, respectively. The ultrafast decay could be due to the smaller 50-100 nm nanowire diameter than the ~93 nm mean free path of carriers in p-GaN at 295 K [22], resulting in a super-efficient carriers extraction to the lateral surface. In addition, with the introduction of cobalt, the carrier decay appears to be hindered, forming a deep tailing that extends up to 70 ps (**Figure S3b**). This is due to the ultrafast photoinduced electron transfer and the formation of a charge-separated state in which the photogenerated holes are localized in the cobalt cluster surface [23]. Since the GaN was magnesium doped, holes will be the majority carriers transferring within GaN nanowires [24]. As previously published studies on Mg-type doped GaN nanowires indicated, the hole concentration in p-type GaN nanowires will be at least one order of magnitude higher than electron concentration [10, 18a]. Thus, holes are more favored to be transferred between p-GaN and Co cluster. We further conducted the excitation intensity dependent TRPL with varied pump power from 120 μW to 1200 μW, as **Figure S15** shown. Both pure p-GaN and $Co_{0.1}$/p-GaN exhibited an increase average decay time with the increase of pump power, indicating the saturated non-radiative recombination centers. This also aligns with the irradiation intensity-dependent productivity experiments as **Figure 2c** shown. Therefore, the high PNOCM activity can be attributed to the critical methane activation and C-C coupling on Co cluster, which are greatly accelerated via the ultrafast photogenerated charge transfer from p-GaN to Co cluster.

10.1002/anie.202500158

RESEARCH ARTICLE

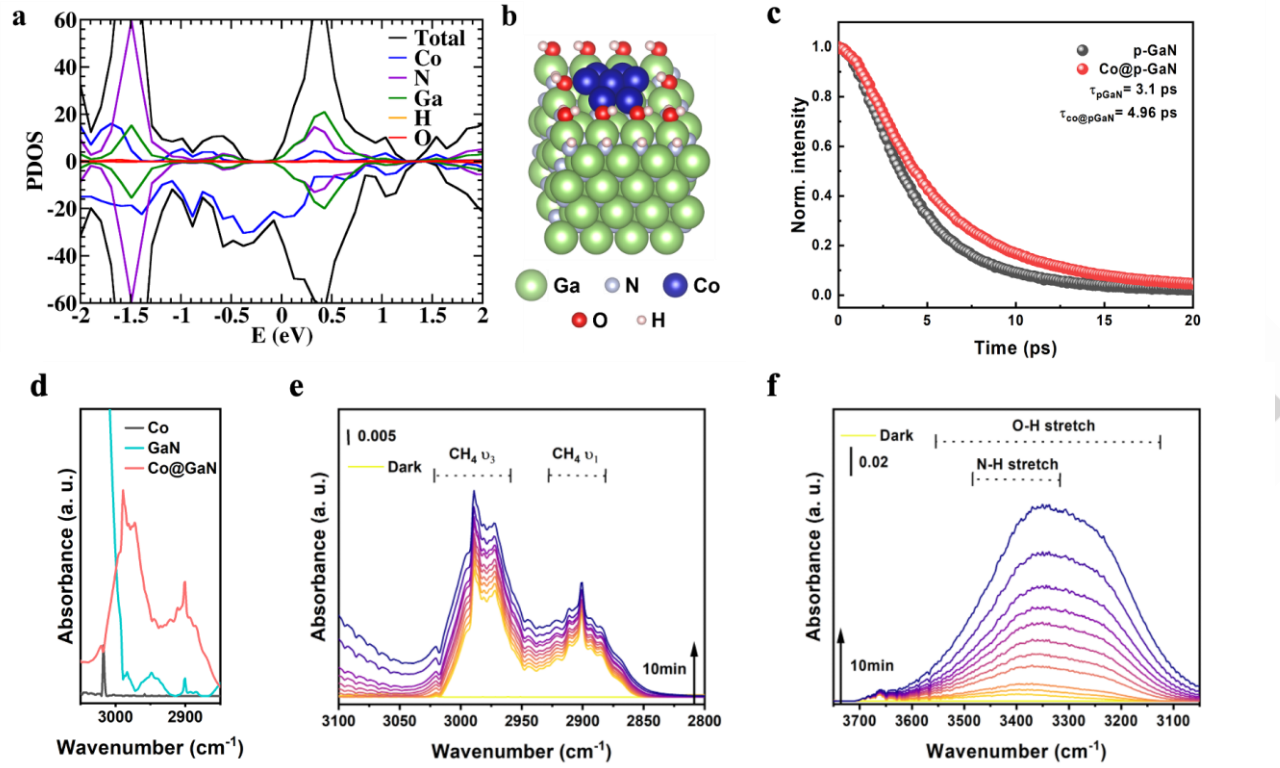

Figure 5. (a) Total Density of states (DOS) and projected density of states (PDOS) of each element around the GaN band gap (Fermi energy E_F = -0.69 eV) of (b) the Co_7-GaN cluster model. Positive density corresponds to the alpha channel and negative density corresponds to the beta channel. (c) Time resolved photoluminescence (TRPL) spectra of $Co_{0.1}$/p-GaN and p-GaN. (d) In situ ATR-FTIR spectra of cobalt metal powder (dark), p-GaN nanowires (pale blue) and cobalt cocatalysts loaded p-GaN nanowires (red) after 10 minutes 365 nm irradiation (3 W, LED) under methane atmosphere. ATR spectrum of CH_4 branches (e) and O-H, N-H branches (f) collected from CH_4/H_2O/GaN nanowires interface under 365 nm (3 W, LED) light illumination in 10min using cobalt cocatalysts.

To further investigate the underlining reaction mechanism of PNOCM, we performed *in situ* the attenuated total reflectance Fourier transform infrared (ATR-FTIR) to observe the interaction between reaction species and metallic cobalt powder, GaN nanowires and $Co_{0.1}$/p-GaN nanowires under reaction conditions (**Figure 5d**). The cobalt metal exhibits a CH_4 adsorption peak at 3018 cm^{-1} and bare GaN nanowires exhibit an intense O-H adsorption peak from 3000 to 3700 cm^{-1}. Bare GaN nanowires also show several CH_4 adsorption peaks with different vibration modes, which are much weaker compared to $Co_{0.1}$/p-GaN. In addition, the water adsorption on $Co_{0.1}$/p-GaN was greatly suppressed, consistent with the DFT calculation predicted. As shown in **Figure 5e**, the peaks at 2989 cm^{-1} and 2900 cm^{-1} were observed on $Co_{0.1}$/p-GaN under irradiation, which could be attributed to the methyl species formed at the initial C-H (ν_{as}/ν_s) activation of methane [25]. This clearly proves the effective adsorption and polarization of these infrared-forbidden free CH_4 molecules at $Co_{0.1}$/p-GaN surface. The polarization of C-H bonds of methane on wurtzite GaN m-plane has been reported before, while it was further enhanced with the addition of cobalt cocatalysts [26]. Furthermore, during the NOCM process, both N-H group and O-H group were formed to compose one mixed peak in **Figure 5f**. The in situ generated N-H and O-H groups in water condition increased with the reaction time, which plays an important role in interacting with methane for lowering the barrier of C–H bond activation on $Co_{0.1}$/p-GaN [1c, 27].

Conclusion

In summary, we have developed a Co cluster triggered GaN nanowires system for PNOCM, which exhibits exceptional activity and stability with minimal coking over extended periods of time. The DFT calculations reveal that NOCM is thermodynamically feasible on cobalt surface, which can be fast accelerated by the ultraefficient charge transfer from GaN to Co cluster. The in-situ ATR-FTIR reveals that the N-H and O-H species formed on GaN surface during reaction plays a synergetic role for activation and polarization of CH_4 molecules. Consequently, very little amount of Co clusters (0.1 wt%) on p-GaN triggered maximum ethane conversion rates of 192.3 mmol g^{-1} h^{-1}, and propane conversion rates at 17.9 mmol g^{-1} h^{-1}, respectively. In addition, the high durability of PNOCM more than 110 h was achieved by suppressing the methane overoxidation on lattice oxygen and surface photocorrosion due to the ultra-stable p-GaN nanowire. These findings highlight the synergistic roles played by GaN and Co clusters for the highly efficient photocatalytic coupling of CH_4.

Acknowledgements

This work was supported by the United States Army Research Office Award W911NF2110337. The authors thank Dr. Peng Zhou for his help with some of the experiments. ZL, JPM, FG and VSB gratefully acknowledge the computation resources from the Yale Center for Research Computing and the National Energy Research Scientific Computing Center (NERSC), a U.S. Department of Energy Office of Science User Facility at Lawrence Berkeley National Laboratory.

Conflict of Interest: Some IP related to this work has been licensed to NX Fuels, Inc. and NS Nanotech, Inc., which were co-founded by Z. Mi. The University of Michigan and Mi have a financial interest in the company.

Keywords: Photocatalytic NOCM • GaN Nanowire • Cobalt metal cluster • Ethane and Propane

[1] a) X. Li, C. Wang, J. Tang, *Nat. Rev. Mater.* **2022**, *7*, 617-632; b) V. L. Sushkevich, D. Palagin, M. Ranocchiari, J. A. van Bokhoven, *Science* **2017**, *356*, 523-527; c) B. An, Z. Li, Z. Wang, X. Zeng, X. Han, Y. Cheng, A. M. Sheveleva, Z. Zhang, F. Tuna, E. J. L. McInnes, M. D. Frogley, A. J. Ramirez-Cuesta, L. S. Natrajan, C. Wang, W. Lin, S. Yang, M. Schröder, *Nat. Mater.* **2022**, *21*, 932-938; d) Z. Fan, W. Xiao, *Angew. Chem. Int. Ed.* **2021**, *60*, 7664-7668.

[2] a) M. Ravi, M. Ranocchiari, J. A. van Bokhoven, *Angew. Chem. Int. Ed.* **2017**, *56*, 16464-16483; b) H. Song, X. Meng, Z.-j. Wang, H. Liu, J. Ye, *Joule* **2019**, *3*, 1606-1636; c) N. Agarwal, S. J. Freakley, R. U. McVicker, S. M. Althahban, N. Dimitratos, Q. He, D. J. Morgan, R. L. Jenkins, D. J. Willock, S. H. Taylor, C. J. Kiely, G. J. Hutchings, *Science* **2017**, *358*, 223-227; d) P. Xie, J. Ding, Z. Yao, T. Pu, P. Zhang, Z. Huang, C. Wang, J. Zhang, N. Zecher-Freeman, H. Zong, D. Yuan, S. Deng, R. Shahbazian-Yassar, C. Wang, *Nat. Commun.* **2022**, *13*, 1375; e) Q. Li, Y. Ouyang, H. Li, L. Wang, J. Zeng, *Angew. Chem. Int. Ed.* **2022**, *61*, e202108069.

[3] a) J. Wortman, V. O. Igenegbai, R. Almallahi, A. H. Motagamwala, S. Linic, *Nat. Mater.* **2023**; b) S. Song, H. Song, L. Li, S. Wang, W. Chu, K. Peng, X. Meng, Q. Wang, B. Deng, Q. Liu, Z. Wang, Y. Weng, H. Hu, H. Lin, T. Kako, J. Ye, *Nat. Catal.* **2021**, *4*, 1032-1042.

[4] L. Yuliati, H. Yoshida, *Chem. Soc. Rev.* **2008**, *37*, 1592-1602.

[5] a) S. F. Moya, R. L. Martins, A. Ota, E. L. Kunkes, M. Behrens, M. Schmal, *Appl. Catal. A.* **2012**, *411-412*, 105-113; b) S. K. Kim, H. W. Kim, S. J. Han, S. W. Lee, J. Shin, Y. T. Kim, *Commun. Chem.* **2020**, *3*, 58; c) L. Guczi, K. V. Sarma, L. Borkó, *Catal. Lett.* **1996**, *39*, 43-47; d) H. Sheng, E. P. Schreiner, W. Zheng, R. F. Lobo, *Chemphyschem* **2018**, *19*, 504-511.

[6] a) Y. Chen, S. Tang, L. Li, X. Liu, J. Liang, *ACS Sustain. Chem. Eng.* **2023**, *11*, 3568-3575; b) Y. Yang, Z. Chai, X. Qin, Z. Zhang, A. Muhetaer, C. Wang, H. Huang, C. Yang, D. Ma, Q. Li, D. Xu, *Angew. Chem. Int. Ed.* **2022**, *61*, e202200567; c) H. Song, H. Huang, X. Meng, Q. Wang, H. Hu, S. Wang, H. Zhang, W. Jewasuwan, N. Fukata, N. Feng, J. Ye, *Angew. Chem. Int. Ed.* **2023**, *62*, e202215057; d) X. Sun, X. Chen, C. Fu, Q. Yu, X.-S. Zheng, F. Fang, Y. Liu, J. Zhu, W. Zhang, W. Huang, *Nat. Commun.* **2022**, *13*, 6677; e) X. Yu, V. L. Zholobenko, S. Moldovan, D. Hu, D. Wu, V. V. Ordomsky, A. Y. Khodakov, *Nat. Energy* **2020**, *5*, 511-519.

[7] a) F. Amano, A. Shintani, K. Tsurui, H. Mukohara, T. Ohno, S. Takenaka, *ACS Energy Lett.* **2019**, *4*, 502-507; b) H. Zhang, W. Zhong, Q. Gong, P. Sun, X. Fei, X. Wu, S. Xu, Q. Zhang, G. Fu, S. Xie, Y. Wang, *Angewandte Chemie International Edition* **2023**, *62*, e202303405.

[8] a) W. Huang, L. Sun, P. Han, J. Zhao, *Journal of Natural Gas Chemistry* **2012**, *21*, 98-103; b) X. Guo, G. Fang, G. Li, H. Ma, H. Fan, L. Yu, C. Ma, X. Wu, D. Deng, M. Wei, D. Tan, R. Si, S. Zhang, J. Li, L. Sun, Z. Tang, X. Pan, X. Bao, *Science* **2014**, *344*, 616-619; c) S. J. Han, S. W. Lee, H. W. Kim, S. K. Kim, Y. T. Kim, *ACS Catalysis* **2019**, *9*, 7984-7997; d) V. Chaudhari, K. Dutta, C.-J. Li, J. Kopyscinski, *Molecular Catalysis* **2020**, *482*, 110606; e) J.-H. Wen, G.-C. Wang, *The Journal of Physical Chemistry C* **2020**, *124*, 13249-13262; f) H. E. Toraman, K. Alexopoulos, S. C. Oh, S. Cheng, D. Liu, D. G. Vlachos, *Chemical Engineering Journal* **2021**, *420*, 130493; g) S. Wu, L. Wang, J. Zhang, *Journal of Photochemistry and Photobiology C: Photochemistry Reviews* **2021**, *46*, 100400; h) W. Zhang, C. Fu, J. Low, D. Duan, J. Ma, W. Jiang, Y. Chen, H. Liu, Z. Qi, R. Long, Y. Yao, X. Li, H. Zhang, Z. Liu, J. Yang, Z. Zou, Y. Xiong, *Nature Communications* **2022**, *13*, 2806; i) H. Zhang, A. Bolshakov, R. Meena, G. A. Garcia, A. I. Dugulan, A. Parastaev, G. Li, E. J. M. Hensen, N. Kosinov, *Angewandte Chemie International Edition* **2023**, *62*, e202306196; j) Z. Chen, Y. Ye, X. Feng, Y. Wang, X. Han, Y. Zhu, S. Wu, S. Wang, W. Yang, L. Wang, J. Zhang, *Nature Communications* **2023**, *14*, 2000; k) M. Zhou, H. Wang, *JACS Au* **2022**, *2*, 188-196; l) T. Zhang, D. Holiharimanana, X. Yang, Q. Ge, *The Journal of Physical Chemistry C* **2020**, *124*, 26722-26729; m) A. Almithn, S. N. Alghanim, A. A. Mohammed, A. K. Alghawinim, M. A. Alomaireen, Z. Alhulaybi, S. S. Hossain, *Catalysts* **2023**, *13*, 531; n) X. Huang, D. Eggart, G. Qin, B. B. Sarma, A. Gaur, J. Yang, Y. Pan, M. Li, J. Hao, H. Yu, A. Zimina, X. Guo, J. Xiao, J.-D. Grunwaldt, X. Pan, X. Bao, *Nature Communications* **2023**, *14*, 5716; o) S. Nachimuthu, H.-J. Lai, Y.-C. Chen, J.-C. Jiang, *Applied Surface Science* **2022**, *577*, 151938; p) J. Lang, Y. Ma, X. Wu, Y. Jiang, Y. H. Hu, *Green Chemistry* **2020**, *22*, 4669-4675; q) T. Zhang, X. Yang, Q. Ge, *Catalysis Today* **2021**, *368*, 140-147.

[9] a) P. Schwach, X. Pan, X. Bao, *Chemical Reviews* **2017**, *117*, 8497-8520; b) Z. Liu, B. Xu, Y.-J. Jiang, Y. Zhou, X. Sun, Y. Wang, W. Zhu, *ACS Environmental Au* **2023**, *3*, 252-276; c) E. R. Januario, P. F. Silvaino, A. P. Machado, J. Moreira Vaz, E. V. Spinace, *Frontiers in Chemistry* **2021**, *9*; d) Z. Zhu, W. Guo, Y. Zhang, C. Pan, J. Xu, Y. Zhu, Y. Lou, *Carbon Energy* **2021**, *3*, 519-540; e) D. Hu, V. V. Ordomsky, A. Y. Khodakov, *Applied Catalysis B: Environmental* **2021**, *286*, 119913.

[10] M. G. Kibria, F. A. Chowdhury, S. Zhao, B. AlOtaibi, M. L. Trudeau, H. Guo, Z. Mi, *Nat. Commun.* **2015**, *6*, 6797.

[11] J. Yin, Z. Yin, J. Jin, M. Sun, B. Huang, H. Lin, Z. Ma, M. Muzzio, M. Shen, C. Yu, H. Zhang, Y. Peng, P. Xi, C.-H. Yan, S. Sun, *Journal of the American Chemical Society* **2021**, *143*, 15335-15343.

[12] a) T. L. Duan, J. S. Pan, D. S. Ang, *Appl. Phys. Lett.* **2013**, *102*; b) W. J. Dong, I. A. Navid, Y. Xiao, J. W. Lim, J.-L. Lee, Z. Mi, *Journal of the American Chemical Society* **2021**, *143*, 10099-10107.

[13] H. J. Mathieu, in *Surface Analysis – The Principal Techniques*, **2009**, pp. 9-45.

[14] a) T. T. D. Nguyen, D. Nguyen, P. P. Vo, H. N. Doan, H. T. N. Pham, V. H. Hoang, K. Tien Le, K. Kinashi, V. T. Huynh, P. T. Nguyen, *J. Mol. Liq.* **2023**, *381*, 121831; b) G. V. Buxton, C. L. Greenstock, W. P. Helman, A. B. Ross, *J. Phys. Chem. Ref. Data* **1988**, *17*, 513-886.

[15] B. Zhang, P. Zhou, Z. Ye, I. A. Navid, Y. Pan, Y. Xiao, K. Sun, Z. Mi, *Nat. Synth.* **2024**.

[16] B. Liu, R. Smith, M. Athanasiou, X. Yu, J. Bai, T. Wang, *Appl. Phys. Lett.* **2014**, *105*, 261103.

[17] a) S. Hoang, P.-X. Gao, *Advanced Energy Materials* **2016**, *6*, 1600683; b) L. Liu, B. Zhang, X. Tan, D. Tan, X. Cheng, B. Han, J. Zhang, *Chem. Commun.* **2020**, *56*, 4567-4570; c) Z. Su, B. Zhang, J. Shi, D. Tan, F. Zhang, L. Liu, X. Tan, D. Shao, G. Yang, J. Zhang, *Sustainable Energy & Fuels* **2019**, *3*, 1233-1238.

[18] a) M. G. Kibria, S. Zhao, F. A. Chowdhury, Q. Wang, H. P. T. Nguyen, M. L. Trudeau, H. Guo, Z. Mi, *Nat. Commun.* **2014**, *5*, 3825; b) W. J. Dong, Z. Ye, S. Tang, I. A. Navid, Y. Xiao, B. Zhang, Y. Pan, Z. Mi, *Advanced Science* **2024**, *11*, 2309548; c) Y. Xiao, X. Kong, S. Vanka, W. J. Dong, G. Zeng, Z. Ye, K.

Sun, I. A. Navid, B. Zhou, F. M. Toma, H. Guo, Z. Mi, *Nat. Commun.* **2023**, *14*, 2047.
[19] a) H. Zhang, P. Sun, X. Fei, X. Wu, Z. Huang, W. Zhong, Q. Gong, Y. Zheng, Q. Zhang, S. Xie, G. Fu, Y. Wang, *Nat. Commun.* **2024**, *15*, 4453; b) J. R. Dunlop, F. P. Tully, *The Journal of Physical Chemistry* **1993**, *97*, 11148-11150; c) F. Amano, K. Beppu, Y. Sakata, *ACS Catalysis* **2024**, *14*, 7788-7794.
[20] J. P. Menzel, W. J. Dong, E. Gruszecki, K. R. Yang, Z. Mi, V. S. Batista, *ACS Catalysis* **2024**, *14*, 13314-13323.
[21] Z. Luo, Y.-K. Peng, H. Xiong, *Chem* **2022**, *8*, 1545-1547.
[22] S. Hafiz, F. Zhang, M. Monavarian, V. Avrutin, H. Morkoç, Ü. Özgür, S. Metzner, F. Bertram, J. Christen, B. Gil, *J. Appl. Phys.* **2015**, *117*.
[23] C. Zhang, G. Lu, Y. Zhang, Z. Fang, H. He, H. Zhu, *The Journal of Chemical Physics* **2022**, *156*.
[24] C. A. Hernández-Gutiérrez, Y. L. Casallas-Moreno, V.-T. Rangel-Kuoppa, D. Cardona, Y. Hu, Y. Kudriatsev, M. A. Zambrano-Serrano, S. Gallardo-Hernandez, M. Lopez-Lopez, *Sci. Rep.* **2020**, *10*, 16858.
[25] Y. Lyu, R. Xu, O. Williams, Z. Wang, C. Sievers, *J. Catal.* **2021**, *404*, 334-347.
[26] L. Li, X. Mu, W. Liu, X. Kong, S. Fan, Z. Mi, C.-J. Li, *Angew. Chem. Int. Ed.* **2014**, *53*, 14106-14109.
[27] a) P. Zhou, S. Tang, Z. Ye, I. A. Navid, Y. Xiao, K. Sun, Z. Mi, *Chemical Science* **2024**, *15*, 1505-1510; b) G. Wang, X. Mu, J. Li, Q. Zhan, Y. Qian, X. Mu, L. Li, *Angew. Chem. Int. Ed.* **2021**, *60*, 20760-20764.

10.1002/anie.202500158

Table of Contents

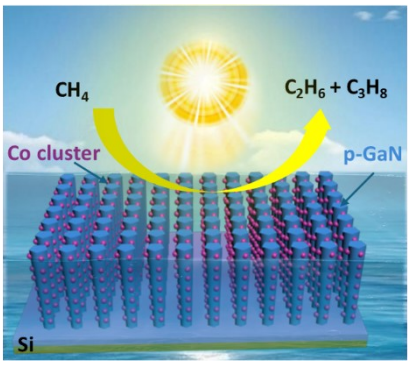

p-Type GaN nanowires with trace metallic cobalt clusters significantly boost the photocatalytic nonoxidative coupling of methane into ethane and propane with exceptional activity, selectivity and stability, which results from the critical methane activation and C-C coupling on Co clusters, accelerated by ultrafast photogenerated charge transfer from p-GaN, with GaN support enhancing methane activation and anti-overoxidation.